Journal of Molecular Structure 1234 (2021) 130146

Contents lists available at ScienceDirect

Journal of Molecular Structure

journal homepage: www.elsevier.com/locate/molstr

Synthesis, X-ray, spectroscopic characterization, Hirshfeld surface analysis, DFT calculation and molecular docking investigations of a novel 7-phenyl-2,3,4,5-tetrahydro-1*H*-1,4- diazepin-5-one derivative

Wedad Al Garadi[a,#], Youness El Bakri[a,b,#,*], Chin-Hung Lai[c,d,*], El Hassane Anouar[e], Lhoussaine El Ghayati[a], Joel T. Mague[f], El Mokhtar Essassi[a]

[a] *Laboratoire de Chimie Organique Hétérocyclique, Centre de Recherche des Sciences des Médicaments, Pôle de Compétences Pharmacochimie, URAC 21, Faculté des Sciences, Université Mohammed V Rabat, Avenue Ibn Battouta, BP 1014, Rabat, Morocco*
[b] *Department of Theoretical and Applied Chemistry, South Ural State University, Lenin prospect 76, Chelyabinsk, 454080, Russian Federation*
[c] *Department of Medical Applied Chemistry, Chung Shan Medical University, Taichung 40241, Taiwan*
[d] *Department of Medical Education, Chung Shan Medical University Hospital, 402 Taichung, Taiwan*
[e] *Department of Chemistry, College of Sciences and Humanities in Al-Kharj, Prince Sattam bin Abdulaziz University, Al-Kharj 11942, Saudi Arabia*
[f] *Department of Chemistry, Tulane University, New Orleans, LA 70118, USA*

ARTICLE INFO

Article history:
Received 25 January 2021
Revised 13 February 2021
Accepted 17 February 2021
Available online 24 February 2021

Keywords:
Crystal structure
Tetrahydrodiazepine
Hirshfeld surface analysis
DFT calculations
Molecular docking

ABSTRACT

The tetrahydrodiazepine ring in the title molecule, $C_{11}H_{12}N_2O$, adopts a twisted envelope conformation. In the crystal, inversion dimers are formed by N–H···O hydrogen bonds which are connected into corrugated layers by N–H···O hydrogen bonds and C–H···π(ring) interactions. However, the Hirshfeld surface analysis indicated that the most important intermolecular interaction for the title compound is the H···H contact. Moreover, the DFT-B3LYP study showed that the title compound should have a slightly different geometry in the gas phase with respect to that in the solid phase. The antitumor activity of the novel tetrahydrodiazepine derivative is investigated by investigating its binding affinity into the active site of Checkpoint Kinase Chk1/SB218078. Docking outputs reveal moderate Checkpoint Kinase inhibition by tetrahydrodiazepine derivative.

1. Introduction

The development of general approaches to rare heterocyclic scaffolds and studies on their structure and reactivity are important in synthetic, theoretical, and medicinal chemistry. The exploration of novel structures in drug discovery has gained increasing interest and relevance [1]. Among the small molecules employed in this field, molecular scaffolds that mimic peptide secondary structures are particularly useful for the identification and development of therapeutic agents [1,2]. For example, 1,4-benzodiazepine is an important scaffold or fragment that has been studied extensively and frequently appears in biologically active molecules and drugs [3]. In particular, a large number of 1,4-benzodiazepines act as anxiolytic, antidepressant, anticonvulsant, and antihypnotic agents [4–7] and some of them exhibit antitumor activity [8,9]. The seven-membered 1,4-diazepin-2-one ring mimics β- and γ-turn secondary structures [10–12] and exhibits anticonvulsant activity [13], antibacterial activity against multidrug-resistant Mycobacterium tubercolosis strains [14], antitumor properties [15], and lymphocyte function-associated antigen-1 (LFA-1) antagonists [16,17]. For these reasons, the development of new strategies for the synthesis of 1,4-diazepin-2-ones is ever evolving. The most reported synthetic approaches to 1,4-benzodiazepine skeletons include reaction of 2-aminobenzoic acids and their derivatives or 2-aminobenzophenones with α-amino acids [18,19], cyclocondensation of 2-halobenzoic acid derivatives or 2-halobenzophenones with diamines [20], and the Pictet-Spengler reaction of *N,N'*-dimethyl-*N*-phenyl-1,2-ethanediamine with aldehydes [21,22]. The diazepinone ring is reported in the literature to be prepared from linear precursors by intramolecular reductive amination [12,23–25], lactam formation [26–28], and transamidation [29]. Also, the preparation of 1,4-diazepin-2-ones involves iminophosphorane intermediates by means of an intramolecular aza-Wittig reaction or hydrolysis of the iminophosphoranes to the corresponding amino derivatives followed by intramolecular cyclocondensation [30]. The limit of these procedures is that they involve some preparative difficulties and require several steps [31–37].

* Corresponding authors.
E-mail addresses: yns.elbakri@gmail.com (Y.E. Bakri), chlai125@csmu.edu.tw (C.-H. Lai).
# Both of these authors contributed equally to this paper

https://doi.org/10.1016/j.molstruc.2021.130146
0022-2860/

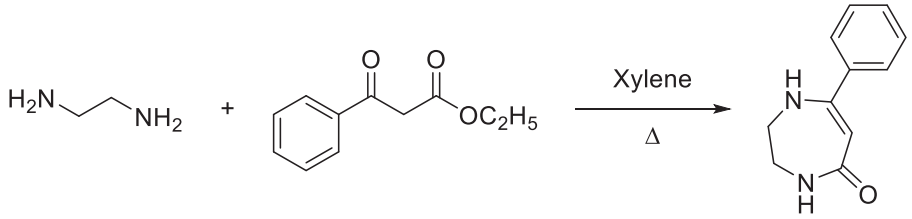

Scheme 1. Schematic representation of the synthesis of the title compound.

2. Experimental and calculated methods

2.1. Synthesis

A solution of (0.1 mol) of ethyl benzoylacetate and 10 mL of xylene was added, dropwise, over 40 min. to a refluxing solution of 0.1 mol ethylene diamine and 100 mL of xylene. During this time an oily layer separated. On cooling, the oil solidified to a hard mass. The xylene layer was decanted and discarded. The solid was suspended in about 100 ml of chloroform and the mixture was filtered. The solid was recrystallized from ethanol to afford the title compound as colorless crystals (Scheme 1).

Thin-layer chromatography and column chromatography were carried out, respectively, on silica plates (Merck 60 F254) and silica gel (Merck 60, 230–400 mesh). The NMR spectra were performed on a Bruker Avance DPX300 instrument. The chemical shifts (δ) are expressed in ppm. Mass spectra were performed on a Perkin-Elmer SCIEX API unit 300. The samples are ionized by the electrospray technique (ESI). Elemental analysis was performed on a Euro EA - CHNSO Elemental Analyzer.

Colorless crystal, Yield: 67%; m.p: 214–216 °C. ^{1}H NMR (600 MHz, DMSO–d_6) δ ppm: 3.41 (m, 4H, CH_2), 4.52 (m, 1H, CH), 7.45–7.50 (m, 5H, CH_{ar}). ^{13}C NMR (151 MHz, DMSO–d_6) δ ppm: 42.41, 47.60, 91.50, 126.95, 128.38, 129.26, 139.45, 152.03, 170.02. HRMS (ESI) Calculated for $C_{11}H_{12}N_2O$: $[M + H^+] = 188.09$, Found: $[M + H^+] = 188.23$. Elemental analysis Calculated: C, 70.19%; H, 6.43%; N, 14.88%; O, 8.50% Found: C, 69.96%; H, 6.76%; N, 15.05%; O, 8.23%.

2.2. X-ray structure determination

A colorless block-like specimen of $C_{11}H_{12}N_2O$, approximate dimensions 0.26 × 0.20 × 0.18 mm^3, was used for the X-ray crystallographic analysis. The X-ray intensity data were measured on a Bruker D8 VENTURE PHOTON 100 CMOS system equipped with an INCOATEC IμS micro–focus source (Cu-K$_\alpha$, λ = 1.54178 Å) and a mirror monochromator.

A hemisphere of data was processed using *SAINT* [38]. The structure (Fig. 1) was solved by direct methods and refined by full-matrix least squares method on F^2 using *SHELXT* and *SHELXL* [39,40]. All the hydrogen atoms were revealed in the first difference Fourier map and were included as riding contributions with isotropic displacement parameters.

At the end of the refinement, the final difference Fourier map showed no peaks of chemical significance and the final value of R1 was 0.0336. The geometrical calculations were carried out using the program PLATON [41]. The molecular and packing diagrams were generated using DIAMOND [42]. The details of the crystal data and structure refinement are given in Table 1.

2.3. DFT details

The structure in the gas phase of the title compound was optimized by means of density functional theory. The DFT calculation was performed by the hybrid B3LYP method, which is based on the idea of Becke and consider a mixture of the exact (HF) and DFT exchange utilizing the B3 functional, together with the LYP correlation functional [43–45] in conjunction with the basis set def2-SVP [46]. After obtaining the converged geometry, the harmonic vibrational frequencies were calculated at the same theoretical level to confirm the number of imaginary frequency is zero for the stationary point. Both the geometry optimization and harmonic vibrational frequency analysis of the title compound were done by the Gaussian 16 program [47]. A more detailed analysis about the electronic property of the title compound was performed by using the NBO 3.1 implemented in the Gaussian 16 program [48].

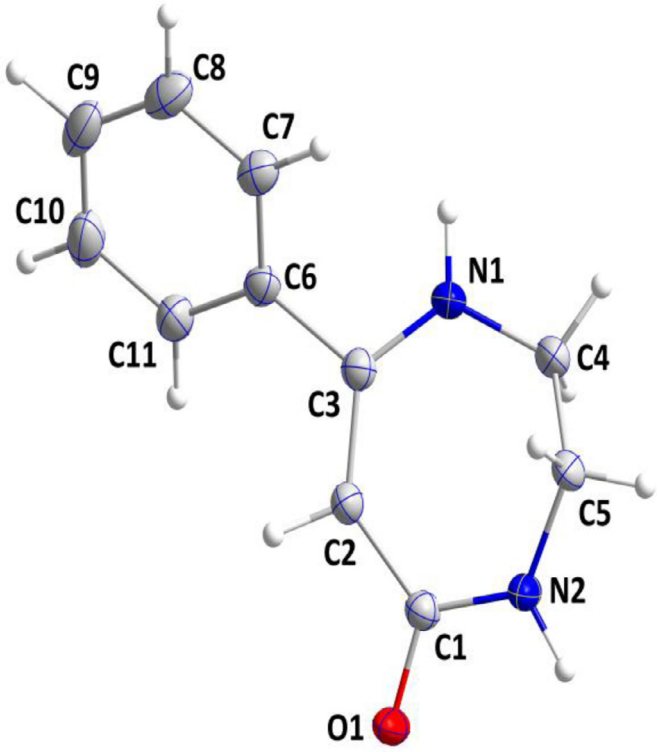

Fig. 1. The title molecule with labeling scheme and 50% probability ellipsoids.

2.4. Hirshfeld surface analysis

Both the definition of a molecule in a condensed phase and the recognition of distinct entities in molecular liquids and crystals are fundamental concepts in chemistry. Based on Hirshfeld's partitioning scheme, Spackman et al. [49] proposed a method to divide the electron distribution in a crystalline phase into molecular fragments [50,51]. Their proposed method partitioned the crystal into regions where the electron distribution of a sum of spherical atoms for the molecule dominates over the corresponding sum of the crystal. Because it derived from Hirshfeld's stockholder partitioning, the molecular surface is named as the Hirshfeld surface. In this study, the Hirshfeld surface analysis of the title compound was performed utilizing the Crystal Explorer program [52].

Table 1
Crystal data and structure refinement details.

Parameter	Value	
CCDC deposit No	1,974,554	
Chemical formula	$C_{11}H_{12}N_2O$	
Formula weight	188.23 g/mol	
Temperature	150(2) K	
Wavelength	1.54178 Å	
Crystal size	0.181 × 0.197 × 0.260 mm^3	
Crystal habit	colorless block	
Crystal system	Monoclinic	
Space group	C 1 2/c 1	
Unit cell dimensions	a = 13.6868(6) Å	$\alpha = 90°$
	b = 13.8189(6) Å	β = 119.166(1)°
	c = 12.1418(5) Å	$\gamma = 90°$
Volume	2005.29(15) $Å^3$	
Z	8	
Density (calculated)	1.247 g/cm^3	
Absorption coefficient	0.657 mm^{-1}	
F(000)	800	
Data collection and structure refinement		
Diffractometer	Bruker D8 VENTURE PHOTON 100 CMOS	
Radiation source	INCOATEC IμS micro-focus source (Cu-K_α (λ = 1.54178 Å))	
Theta range for data collection	4.89 to 72.23°	
Index ranges	$-16 \le h \le 16$, $-15 \le k \le 17$, $-14 \le l \le 14$	
Reflections collected	7515	
Independent reflections	1942 [$R(int)$ = 0.0290]	
Coverage of independent reflections	98.1%	
Absorption correction	multi-scan	
Max. and min. transmission	0.8900 and 0.8480	
Refinement method	Full-matrix least-squares on F^2	
Refinement program	*SHELXL-2018/1* [39,40]	
Function minimized	$\Sigma w(F_o^2 - F_c^2)^2$	
Data/restraints/parameters	1942 / 0 / 176	
Goodness-of-fit on F^2	1.060	
Final R indices	1807 data; $I > 2\sigma(I)$	$R1$ = 0.0336, $wR2$ = 0.0823
	all data	$R1$ = 0.0355, $wR2$ = 0.0838
Weighting scheme	$w = 1/[\sigma^2(F_o^2)+(0.0344P)^2 + 1.2724P]$	
	where $P=(F_o^2+2F_c^2)/3$	
Extinction coefficient	0.0041(3)	
Largest diff. peak and hole	0.217 and −0.177 e$Å^{-3}$	
R.M.S. deviation from mean	0.038 e$Å^{-3}$	

2.5. Molecular docking study

The antitumor activity of tetrahydrodiazepine derivative is investigated using molecular docking study. The Checkpoint Kinase Chk1/SB218078 is chosen a target enzyme (pdb code 1NVS). The intermolecular interactions between the docked compound and the active residues of the target enzyme have been determined using Autodock package [53]. The starting geometries of Checkpoint Kinase Chk1/SB218078 and its original docked ligand were download from the RCSB data bank web site (PDB code 1NVS) [54]. Water molecules were removed; polar hydrogen atoms and Kollman charge were added to the extracted receptor using the automated tool in AutoDock Tools 4.2. The active site is identified based on co-crystallized receptor-ligand complex structure of Checkpoint Kinase Chk1/SB218078 [54]. The re-docking of the original ligand acetohydroxamic acid into the active site is well reproduced with a RMSD value less than 0.94 Å. The docking calculations have been carried out using an Intel (R) Core (TM) i5–3770 CPU @ 3.40 GHz workstation.

3. Results and discussion

3.1. Structure description

The tetrahydrodiazepine ring adopts a twisted envelope conformation with Cremer-Pople puckering parameters Q(2) = 0.5025(12) Å, Q(3) = 0.3729(12) Å, φ(2) = 52.83(14)° and φ(3) = 140.85(19)° [55]. The total puckering amplitude is 0.6757(13) Å. The C6···C11 benzene ring is inclined to the mean plane defined by N1/C1···C4 (deviation from mean plane: −0.0220(5) Å (C1); 0.0300(8) Å (C2); r.m.s. deviation 0.0213) by 43.55(4)° while the inclination to the mean plane of the full diazepine ring is 41.46(6)°. The bond distances and the interbond angles are as expected (Table S3 in the supporting information). For example, the N1—C4 and N2—C5 distances (1.4438(14) and 1.4487(13) Å) are significantly longer than the N1—C3 and N2—C1 distances (1.3473(14) and 1.3426(13) Å) due to the sp^2 hybridization of the latter carbon atoms. In the crystal, N2—H2A···O1 hydrogen bonds (Table 2) form inversion dimers which are linked into corrugated sheets parallel to the bc plane by N1–H1···O1 hydrogen bonds and C5—H5A···$Cg1$ and C5—H5B···$Cg1$ interactions (Table 2 and Figs. 2 and 3).

Table 2
Hydrogen-bond geometry (Å, °).

D–H···A	D–H	H···A	D···A	D–H···A
N2–H2A···O1^{i}	0.947(16)	1.913(16)	2.8591(12)	177.0(13)
N1–H2···O1^{ii}	0.905(16)	1.924(16)	2.7937(12)	160.4(14)
C5–H5A···Cg1^{iii}	0.996(13)	2.755(14)	3.6160(13)	145.0(12)
C5–H5B···Cg1^{iv}	1.019(14)	2.970(15)	3.7285(15)	131.9(10)

Symmetry codes: (i) $-x + 1/2, -y + 1/2, -z + 1$; (ii) $x, -y + 1, z - 1/2$; (iii) $-x + 1/2, y - 1/2, -z + 1/2$; (iv) $-x + 1, -y + 1, -z + 1$.

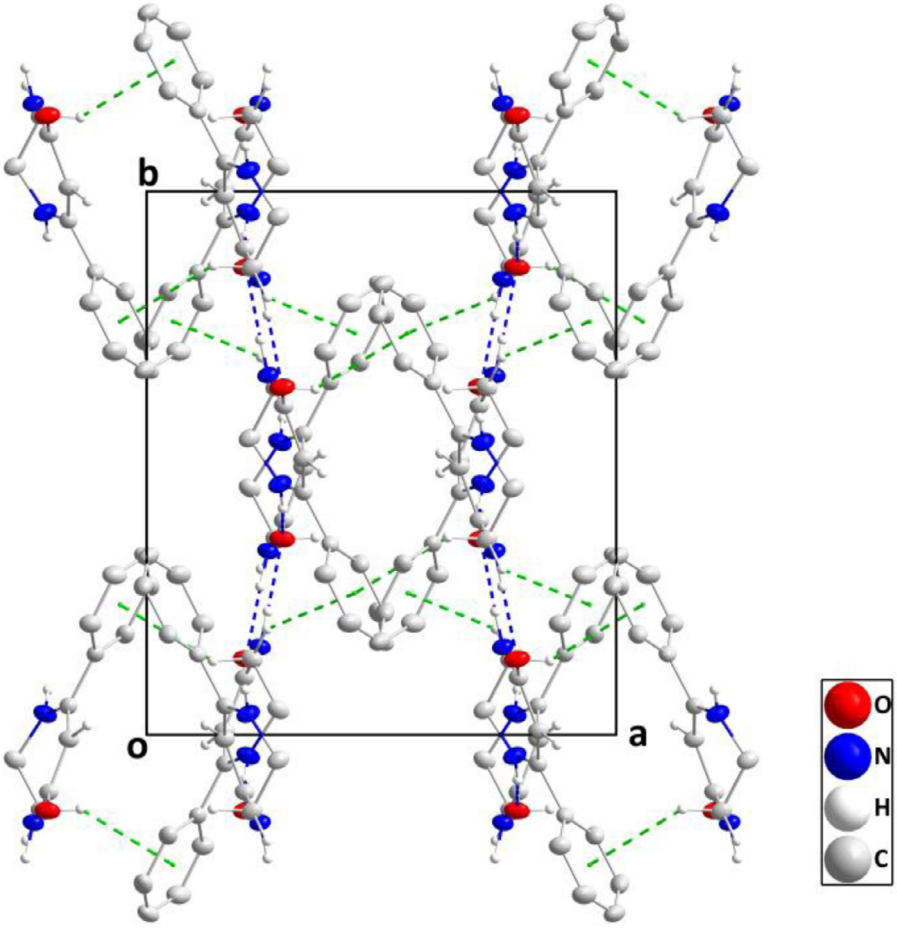

Fig. 2. Packing viewed along the *c*-axis direction with N–H···O hydrogen bonds shown by blue dashed lines. The C–H···π(ring) interactions are shown by green dashed lines.

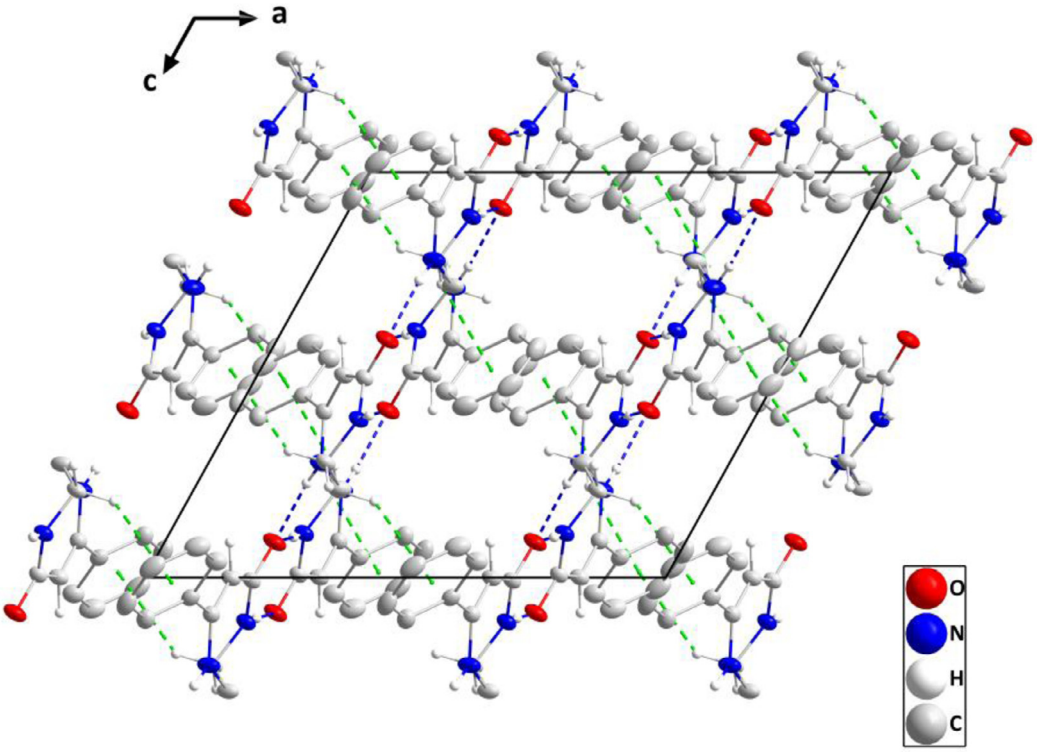

Fig. 3. Packing viewed along the *b*-axis direction with intermolecular interactions depicted as in Fig. 2.

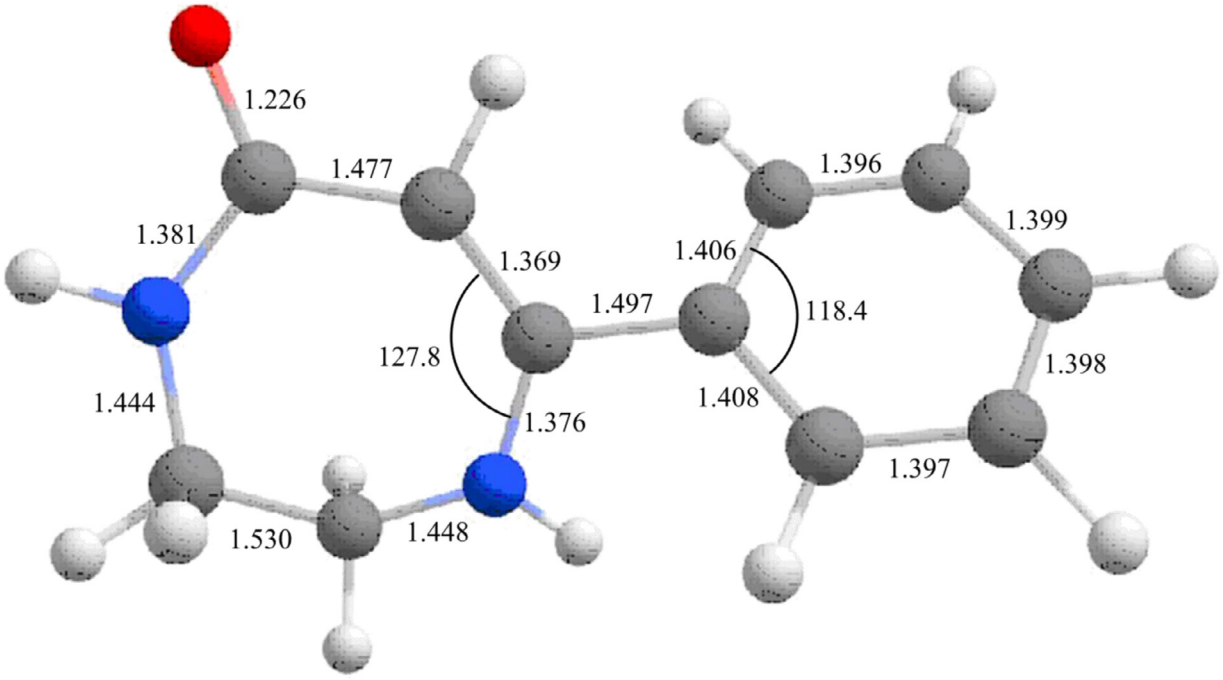

Fig. 4. The B3LYP-optimized geometry of the title compound (bond lengths in Å, bond angles in°).

Table 3
The B3LYP-optimized, and the X-ray structural parameters for the title compound (The atomic designations can be seen in Fig. 1; bond lengths in Å, bond and dihedral angles in°).

	B3LYP	X-ray
C3-C6	1.497	1.4962(14)
C6-C7	1.408	1.3960(15)
C7-C8	1.397	1.3908(17)
C8-C9	1.398	1.383(2)
C3-N1	1.376	1.3473(14)
N1-C4	1.448	1.4438(14)
C4-C5	1.530	1.5193(15)
C5-N2	1.444	1.4487(13)
N2-C1	1.381	1.3426(13)
C1-C2	1.477	1.4547(15)
C2-C3	1.369	1.3715(14)
C1-O1	1.226	1.2633(12)
∠C7-C6-C11	118.4	118.79(10)
∠N1-C3-C2	127.8	127.67(10)
∠N1-C3-C6-C7	−40.05	−41.72(14)
∠C3-N1-C4-C5	−47.60	−45.60(15)

3.2. The comparison between the gas-phase geometry and the solid-phase one

The B3LYP-optimized geometry of the title compound is depicted in Fig. 4 and the bond distance and interbond angles obtained from this optimization are compared to the experimental (X-ray) values for the title compound in Table 3. It is evident from Table 3 that the B3LYP-optimized geometry shows little deviation from the experimental geometry. To quantify the difference between the calculated and experimental geometries, the structure comparer contained in the ChemCraft program was used to obtain their root-mean-square deviations (RMSD) [56]. A weighted RMSD of 0.1089 was obtained to indicate that the optimization gave an RMSD of 0.1496, 0.0480, 00,830, and 0.0301 for H atoms, C atoms, N atoms, and O atoms, respectively.

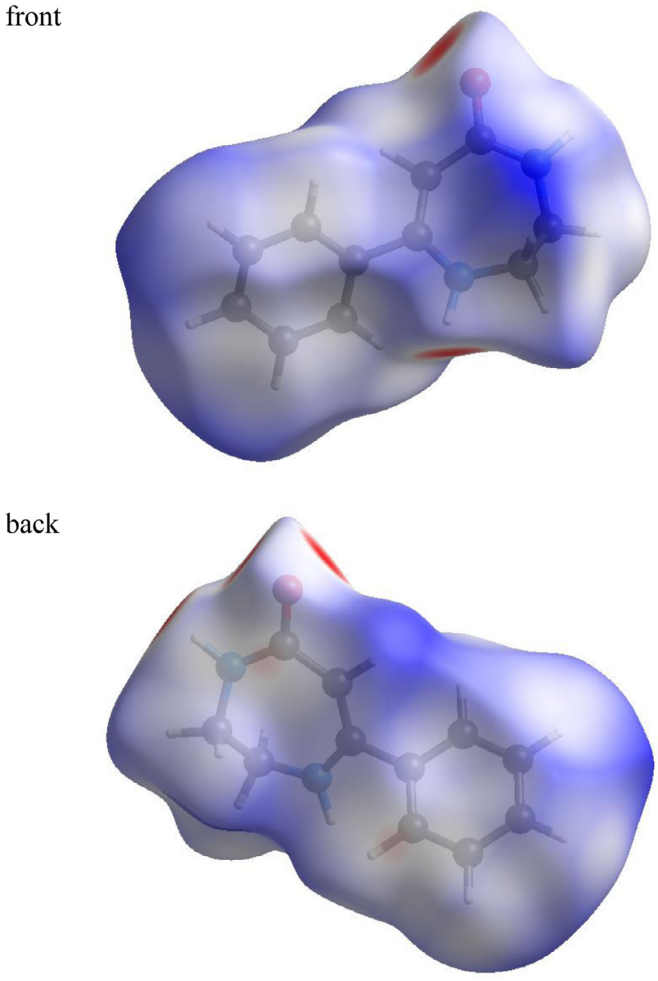

Fig. 5. The d_{norm} Hirshfeld surface of the title compound (red: negative, white: zero, blue: positive; scale: −0.6042 to 1.9277 a.u.).

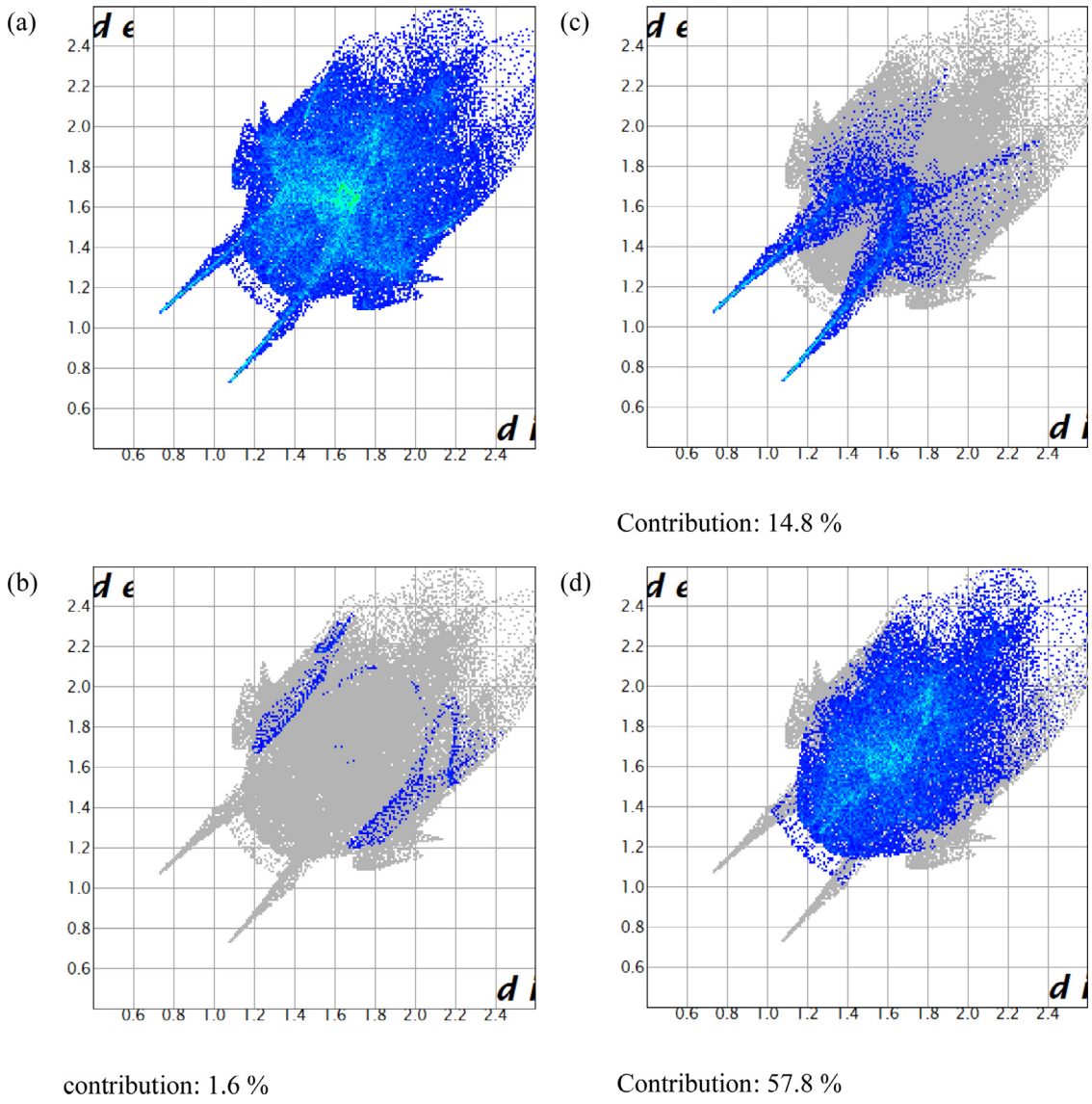

Fig. 6. The 2D fingerprint plot of the title compound (a) full, (b) resolved by the H•••O contacts, (c) resolved by the H···N contacts, (d) resolved by the H···H contacts.

3.3. The Hirshfeld analysis of the title compound

The standard resolution molecular Hirshfeld surface (d_{norm}) of the title compound is depicted in Fig. 5. The surface is shown as transparent so the molecular moiety can be visualized in a similar orientation for all the structures around which they were calculated. The 3D d_{norm} surface can be used to identify very close intermolecular interactions being negative (positive) when intermolecular contacts are shorter (longer) than the sum of the van der Waals radii. The d_{norm} value is mapped onto the Hirshfeld surface with the red regions representing closer contacts with a negative d_{norm} value while the blue regions represent longer contacts with a positive d_{norm} value. The white regions represent contacts equal to the sum of the van der Waals radii and have a d_{norm} value of zero. As depicted in Fig. 5, the important interactions in the title compound may be H···O and H···N hydrogen bonds. In order to understand the relative importance of H···O hydrogen bonds over H···N hydrogen bonds, we calculated the 2D fingerprint plots for the title compound.

The 2D fingerprint plots (Fig. 6) highlight particular atom pair contacts and enable the separation of contributions from different interaction types that overlap in the full fingerprint. Using the standard 0.6–2.6 a.u. view with the d_e and d_i distance scales displayed on the graph axes and including the reciprocal contacts, we found the most important interaction involving hydrogen in the title compound was the H···H contact. The contribution of the H···O, H···N, and H···H contacts are 14.8%, 1.6%, and 57.8%, respectively.

3.4. Frontier molecular orbitals analysis

The important aspect of the frontier molecular orbital theory is the focus on the highest occupied and lowest unoccupied molecular orbitals (HOMO and LUMO). Instead of thinking about the total electron density in a nucleophile, the localization of the HOMO orbital should be considered because electrons from this orbital have the most chance to participate in the nucleophilic attack, while a site where the lowest unoccupied orbital is localized is a good electrophilic site. The frontier orbital of the title compound was further investigated in this study and its HOMO and LUMO were depicted in Fig. 7. As depicted in Fig. 7, the electron density of its HOMO was mostly distributed in the diazepanone moiety, while that of its LUMO was mostly distributed over the phenyl ring.

Furthermore, the quantum chemistry descriptors (chemical hardness η, softness S, electronegativity χ and electrophilicity ω)

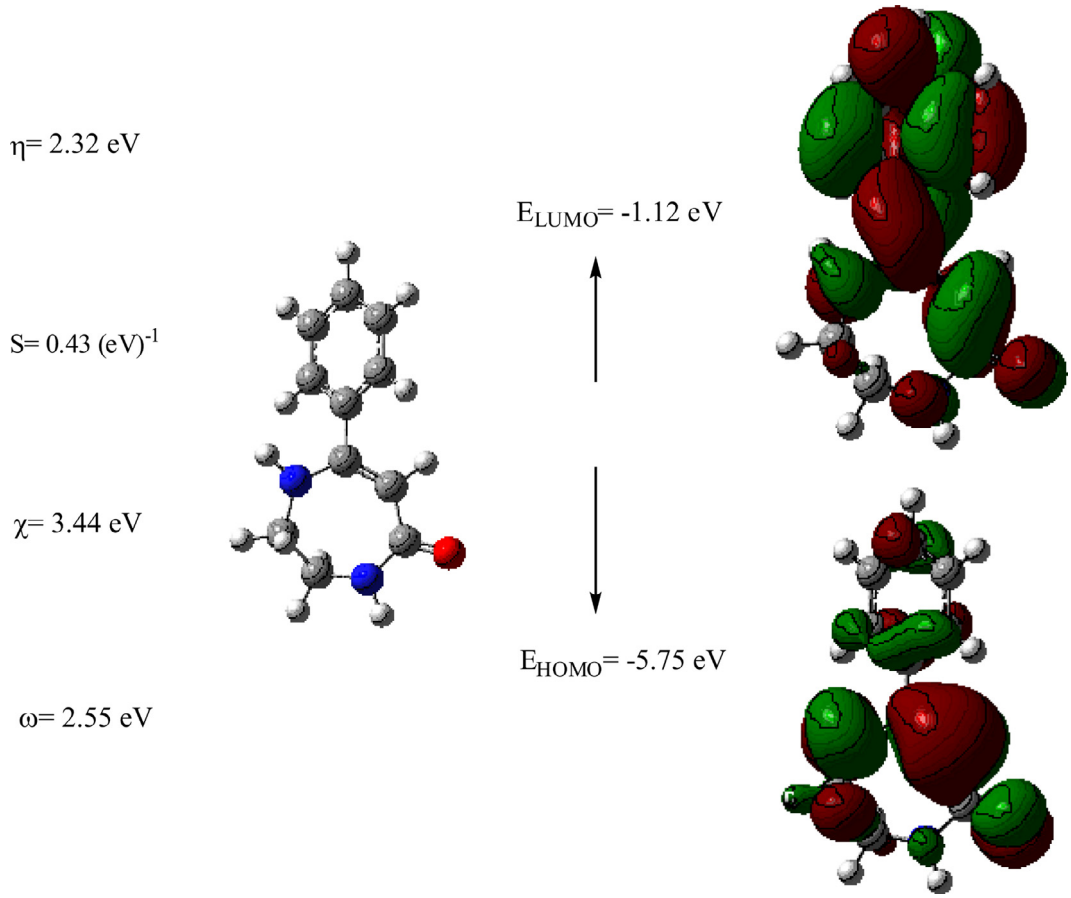

Fig. 7. Optimized structure, quantum parameters and frontier molecular orbitals of title compound.

derived from the conceptual Density Functional Theory of the titled compound were also listed in Fig. 7. The conceptual DFT (CDFT) is a branch of DFT and aims to provide an accurate explanation of some frequently mentioned concepts such as electronegativity and softness. Therefore, CDFT can make some empirical principles, for example, the electronegativity equalization principle, the hard and soft acid-base principle, the maximum hardness principle to have a wider range of applications. In advance accordance to Koopmans' theory, the vertical ionization potential (I), and electron affinity (EA) of a molecule is:

$$\begin{aligned} I &= -E_{HOMO} \\ EA &= -E_{LUMO} \end{aligned} \quad (1)$$

Then, the global chemical reactivity parameters such as the chemical hardness (η), softness (S), electronegativity (χ), and electrophilicity (ω) can be represented as

Chemical hardness is an important feature of chemical species and can be defined as the resistance of atoms, ions or molecules to deform or polarize their electron clouds. The harder a molecule, the greater its ability to prevent its electron cloud from twisting or polarizing. Softness is closely related to reactivity. The softer a molecule, the greater its chemical reactivity. In a molecule, the electronegativity of an atom or a functional group is its ability to attract the bonding electrons to itself. The greater the electronegativity of an atom or functional group, the stronger its ability to attract bonding electrons. Electrophilicity can be regarded as the size of the reactivity of an electron-deficient system with a nucleophile. The greater the electrophilicity of an electron-deficient molecule, the greater its reactivity with a nucleophile [57]. Based on the analysis the frontier orbital, the phenyl ring should be the electrophilic site in the titled compound.

3.5. Molecular electrostatic potential (MEP)

MEPs are fundamentally measures of the interaction strength of the nearby charges, nuclei and electrons at a particular position and thus enabling us to visualize the charge distribution and charge-related characteristics of molecules. In order to make data of the electrostatic potential easy to interpret, a visual representation with a chromatogram is used. Generally, red represents the lowest electrostatic potential value and may be attacked by electrophiles. On the contrary, blue represents the highest electrostatic potential and may be attacked by nucleophiles. The full density matrix is used to generate the total density of the title compound and the resulting MEP is mapped on its surface (Fig. 8). As depicted in Fig. 8, the oxygen atom of the C=O group in the title compound is responsible for the nucleophilic attack due to the fact that it has the largest electronegativity among all kinds of atoms in the title compound. Moreover, MEP also shows the two N–H groups in the title compound could act as the hydrogen bonding donors.

3.6. The results of the NBO analysis

Although some evidences showed that the Mulliken charge displacement around molecular site is useful tool to find out the cause of inducement of drug potential [58], however, Finkelmann et al. compared several partial atomic charge schemes and showed that the NPA charges is a good choice for molecular modeling and design [59]. Therefore, the results of the natural population analysis about the title compound was summarized in Fig. 9. As depicted in Fig. 9, the N1 atom (See the atomic designation in Fig. 1) bears the most negative charge and should be

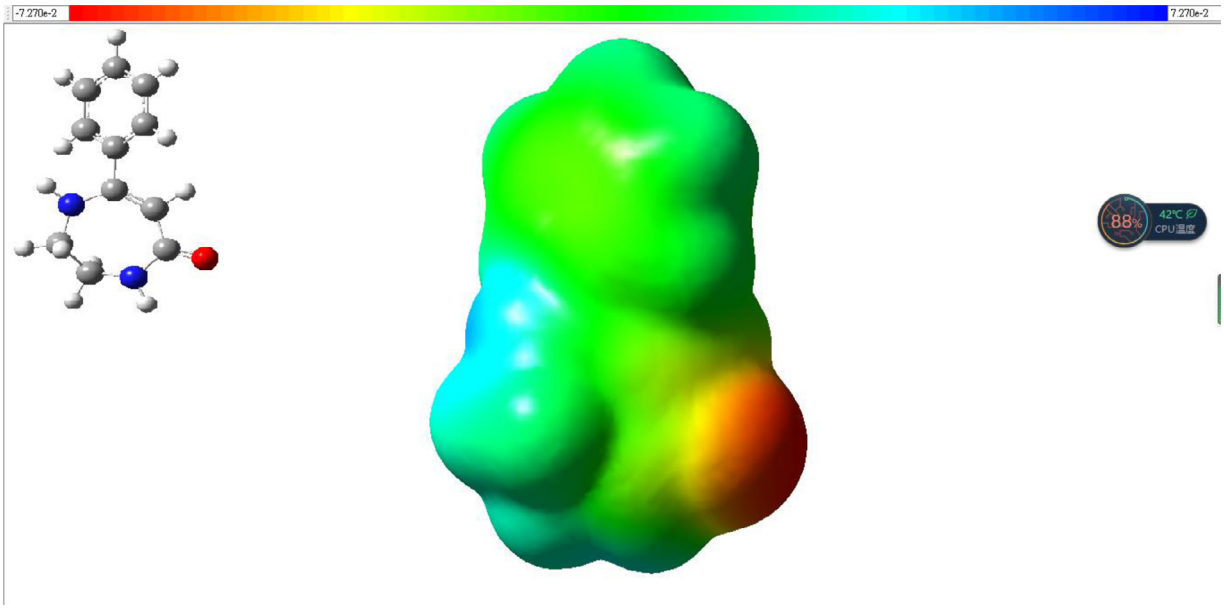

Fig. 8. Molecular Electrostatic Potential (MEP) map of the investigated molecule (the isodensity value = 0.004 a.u.).

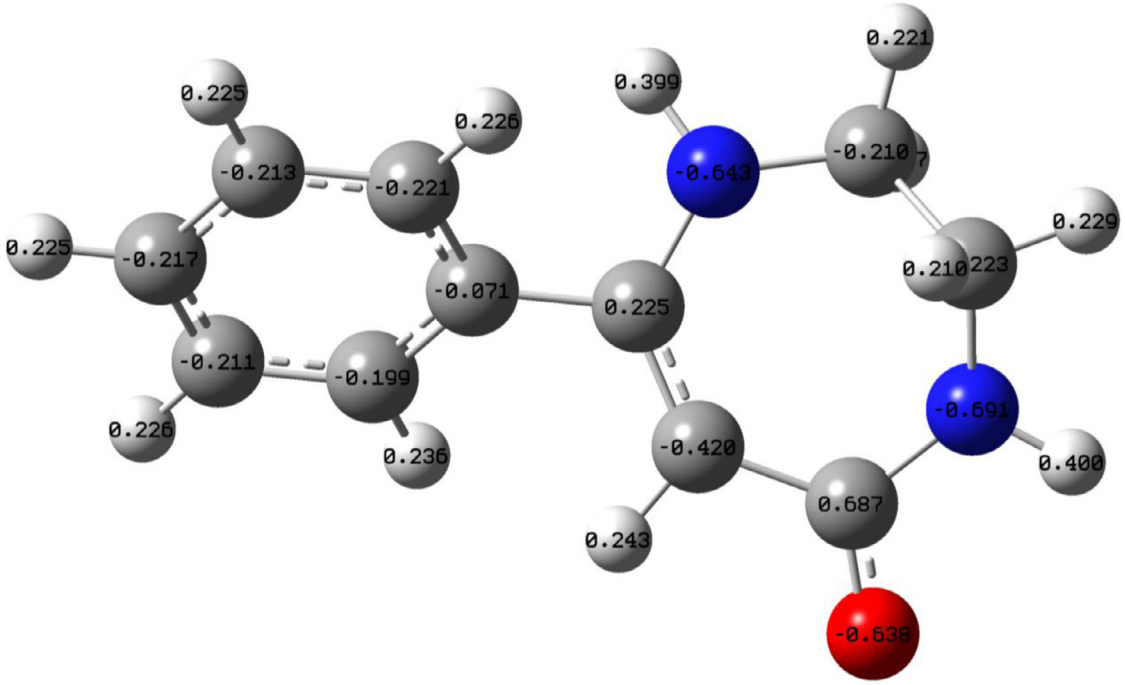

Fig. 9. The results of the natural population analysis.

the most susceptible to the electrophilic attack among the atoms in the title compound. As a hydrogen bond forms, there should be an orbital interaction between the nonbonding orbital of the hydrogen-bonded acceptor (n_A) and the antibonding orbital of the H-Donor bond ($\sigma_{H\text{-}D}^*$). Therefore, the bond strength or bond order of $\sigma_{H\text{-}D}^*$ should be weakened (decreased) due to such orbital interaction. If the stronger the $n_A \cdots \sigma_{H\text{-}D}^*$ orbital interaction, the stronger the hydrogen bond D–H···A. The result of the NBO analysis shows that there should be three strong hydrogen bonds in the title compound which its $E^{(2)}(n_A \cdots \sigma_{H\text{-}D}^*) > 0.5$ kcal/mol. They are C4-H···N1, C4-H'···N1, and C5-H···N2 (See the atomic designations in Fig. 1). The related NBO results are summarized as Table 4 shows.

3.7. Molecular docking analysis

The ability of the novel tetrahydrodiazepine derivative to inhibit Checkpoint Kinase Chk1/SB218078 is estimated by predicting the binding energy of the stable complex compound- Checkpoint Kinase, number of conventional intermolecular hydrogen bonding established between the synthesized compound and active site residues of Checkpoint Kinase Chk1/SB218078. Indeed, the formed complex displayed a negative binding energy of −4.67 kcal/mol, which is a signpost that the inhibition of Checkpoint Kinase Chk1/SB218078 is thermodynamically favorable. Docking results reveal that the binding interactions are mainly of π-type (Fig. 10). Indeed, three π-alkyl interactions are formed between the aro-

Table 4
The results of the NBO analysis.

The type of n_A	The electron configuration of n_A	The type of orbital interaction	$E^{(2)}$ (in kcal/mol)	The occupancy of $\sigma_{H\text{-}D}{}^{*}$	The bond order of $\sigma_{H\text{-}D}{}^{b}$
LP1 of N1[a]	s(3.15%)p(96.84%)d(0.01%)	LP(N1)-σ^{*}(C4-H)	8.46	0.02904	0.9068
LP1 of N1[a]	s(3.15%)p(96.84%)d(0.01%)	LP(N1)-σ^{*}(C4-H')	1.25	0.01142	0.9200
LP1 of N2[a]	s(1.24%)p(98.75%)d(0.01%)	LP(N2)-σ^{*}(C5-H)	8.47	0.02851	0.7485

Please see the atomic designations in Fig. 1.
b. The listed values were the atom-atom overlap-weighted NAO bond order.

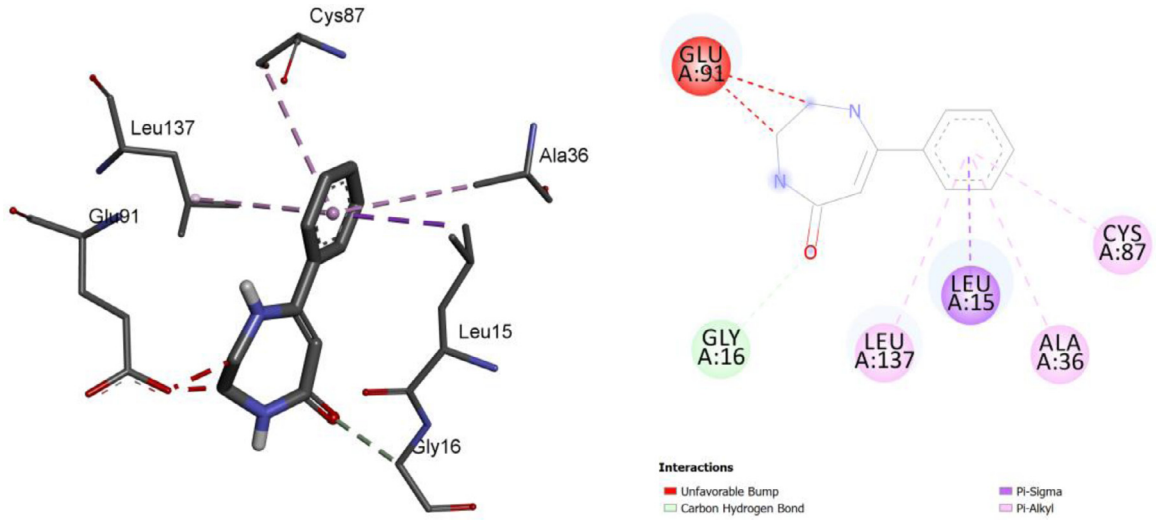

Fig. 10. 3D (left) and 2D (left) intermolecular interactions of name of compound and active amino acids of Checkpoint Kinase Chk1/SB218078.

matic ring of tetrahydrodiazepine derivative and Leu-A137, Ala-A36, and Cys-A87; and π-σ interaction between sigma bonds of the aromatic ring and Leu-A15 (Fig. 10). Further, a carbon hydrogen bond is formed between the methine of Gly16 and the keto group of the seven-member ring of tetrahydrodiazepine derivative of a distance 3.05 Å (Fig. 10).

Conclusion

In this study, an efficient and atom-economic method to synthesize the diazepinone derivatives. The synthesized compound, $C_{11}H_{12}N_2O$ was further investigated by X-ray crystallograpical, DFT-B3LYP, and Hirshfeld surface analysis studies. In the crystal, the title compound form inversion dimers by N–H···O hydrogen bonds which are connected into corrugated layers by N–H···O hydrogen bonds and C–H···π(ring) interactions. However, the Hirshfeld surface analysis indicated that the most important intermolecular interaction for the title compound is the H···H contact. Moreover, the DFT-B3LYP study showed that the title compound should have a slightly different geometry in the gas phase with respect to that in the solid phase. The molecular docking study expected moderate affinity of tetrahydrodiazepine to bind to Checkpoint Kinase Chk1/SB218078 active site, and that binding interactions are mainly of π-type.

Author contribution statement

Wedad Al Garadi: Synthesized and characterized the title molecule.

Youness El Bakri: Data curation, Wrote the paper; Final approval of the version submitted.

Chin-Hung Lai: Writing-reviewing and performed quantum-chemical calculations, analyzed and interpreted the data

El Hassane Anouar: Writing and performed quatum-chemical calculations, analyzed and interpreted the data.

Lhoussaine El Ghayati: Visualization, Invistigation and data curation.

Joel T. Mague: Performed the X-ray experiments and analyzed and interpreted the data.

El Mokhtar Essassi: Conceptualization and supervision.

Declaration of Competing Interest

There are no conflicts to declare.

Acknowledgements

The support of NSF-MRI Grant # 1228232 for the purchase of the diffractometer and Tulane University for support of the Tulane Crystallography Laboratory are gratefully acknowledged. We also thank the National Center for High-performance Computing (Taiwan) for providing computing time. The authors also gratefully acknowledge Mohammed V University (Morocco) for the financial assistance and facilitation to facilitate this study. Special thanks are also due to Reviewers and Editors for their very helpful suggestions and comments.

References

[1] D.A. Horton, G.T. Boune, M.L. Smythe, Chem. Rev. 103 (2003) 893.
[2] B.E. Evans, K.E. Rittle, M.G. Block, R.M. DiPardo, R.M. Freidinger, W.L. Whitter, G.F. Lundell, D.F. Veber, P.S. Anderson, R.S.L. Chang, V.J. Lotti, D.J. Cerino, T.B. Chen, P.J. Kling, K.A. Kunkel, J.P. Springer, J. Hirshfield, J. Med. Chem. 31 (1988) 2235.
[3] L. Costantino, D. Barlocco, Curr. Med. Chem. 13 (2006) 65.
[4] D. Berezhnoy, T.T. Gibbs, D.H. Farb, Mol. Pharmacol. 76 (2009) 440.
[5] B. Kadriu, A. Guidotti, È. Costa, M. John, J. Auta, Toxicol. Sci. 120 (2011) 136.
[6] M.T. Bianchi, Curr. Neuropharmacol. 8 (2010) 10.
[7] C. Alhambra, C. Becker, T. Blake, A.H-F. Chang, J.R.Jr. Damewood, T. Daniels, B.T. Dembofsky, D.A. Gurley, J.E. Hall, K.J. Herzog, C.L. Horchler, C.J. Ohnmacht, R.J. Schmiesing, A. Dudley, M. Ribadeneira, K.S. Knappenberger, C. Maciag, M.M. Stein, M. Chopra, X.F. Liu, E.P. Christian, J.L. Arriza, M.J. Chapdelaine, Bioorg. Med. Chem. 19 (2011) 2927.
[8] S.R.D. Johnston, Drugs 6 (2003) 72.

[9] K.M. Rahman, H. Vassoler, C.H. James, D.E. Thurston, Med. Chem. Lett. 1 (2010) 29.
[10] I.S. Weitz, M. Pellegrini, D.F. Mierke, M. Chorev, J. Org. Chem. 62 (1997) 2527.
[11] S.K. Ramanathan, J. Keeler, H.-.L. Lee, D.S. Reddy, G. Lushington, J. Aube, Org. Lett. 7 (2005) 1059.
[12] H. Iden, W.D. Lubell, Org. Lett. 8 (2006) 3425.
[13] K.S. Keshava Murthy, E.E. Knaus, Drug. Dev. Res. 46 (1999) 155.
[14] S. Hirano, S. Ichikawa, A. Matsuda, J. Org. Chem. 73 (2008) 569.
[15] K.J. Isono, J. Antibiot. 41 (1988) 1711.
[16] S. Wattanasin, R. Albert, C. Ehrhardt, D. Roche, M. Sabio, U. Hommel, K. Welzenbach, G. Weitz-Schmidt, Biorg. Med. Chem. Lett. 13 (2003) 499.
[17] S. Wattanasin, J. Kallen, S. Myers, Q. Guo, M. Sabio, C. Ehrhardt, R. Albert, U. Hommel, K. Welzenbach, G. Weitz-Schmidt, Biorg. Med. Chem. Lett. 15 (2005) 1217.
[18] A. Nadin, J.M. Sanchez Lopez, A.P. Owens, D.M. Howells, A.C. Talbot, T. Harrison, J. Org. Chem. 68 (2003) 2844.
[19] S. Marcaccini, M. Miliciani, R. Pepino, Tetrahedron Lett. 46 (2005) 711.
[20] W. Ho, M.J. Kukla, H.J. Breslin, D.W. Ludovici, P.P. Grous, C.J. Diamond, M. Miranda, J.D. Rodgers, C.Y. Ho, E. De Clercq, R. Pauwels, K. Andries, M.A.C. Janssen, P.A.J. Janssen, J. Med. Chem. 38 (1995) 771.
[21] A.R. Katritzky, Y.-J. Xu, H.-Y. He, J. Chem. Soc. Perkin Trans. 1 2002 (2002) 592.
[22] G.S. Welmaker, J.E. Sebalski, Tetrahedron Lett. 45 (2004) 4851.
[23] N. Nakajima, T. Isobe, S. Irisa, M. Ubukata, Heterocycles 59 (2003) 107.
[24] H.S. Iden, W.D. Lubell, J. Org. Chem. 72 (2007) 8980.
[25] H.S. Iden, W.D. Lubell, J. Comb. Chem. 10 (2008) 691.
[26] L.W.A. Van Berkom, R. De Gelder, H.W. Sheeren, Eur. J. Org. Chem. 5 (2005) 907.
[27] C. Gravier-Pelletier, I. Charvet, Y.Le Merrer, J.C. Depezay, J. Carbohydr. Chem. 16 (1997) 129.
[28] J. Balsells, M. Waters, K. Hansen, G.R. Kieczykowski, Z.J. Song, Synthesis 18 (2007) 2779.
[29] M. Alajarín, A. Vidal, F. Tovar, Tetrahedron 61 (2005) 1531.
[30] M.K. Vokv, N.M. Golovach, V.A. Sukach, O.N. Chernyuk, O.V. Manoilenko, Russ. J. Org. Chem. 46 (2010) 480.
[31] Y. El Bakri, E.H. Anouar, I. Marmouzi, K. Sayah, Y. Ramli, M.E.A. Faouzi, E.M. Essassi, J.T. Mague, J. Mol. Model. 24 (2018) 1.
[32] Y. El Bakri, I. Marmouzi, M. El Jemli, E.H. Anouar, S. Karthikeyan, A. Harmaoui, M. El Abbes Faouzi, J.T. Mague, E.M. Essassi, Bioorg. Chem. 92 (2019) 103193.
[33] I. Rayni, Y. El Bakri, C.-.H. Lai, A. Ben Ali, E.M. Essassi, J.T. Mague, J. Chem. Cryst. 50 (2020) 330.
[34] Y. El Bakri, C.-.H. Lai, J. Sebhaoui, A. Ben Ali, E.M. Essassi, J.T. Mague, J. Mol. Struct. 1184 (2019) 12.
[35] I. Chakib, Y. El Bakri, C.-.H. Lai, L. Benbacer, A. Zerzouf, E.M. Essassi, J.T. Mague, J. Mol. Struct. 1198 (2019) 126910.
[36] Y. El Bakri, S. Karthikeyan, E.H. Anouar, J. Sebhaoui, A. Ben Ali, L. El Ghayati, E.M. Essassi, J.T. Mague, J. Biomol. Struct. Dyn. (2019), doi:10.1080/07391102.2019.1662848.
[37] Y. El Bakri, C.-.H. Lai, J. Sebhaoui, A. Ben Ali, Y. Ramli, E.M. Essassi, J.T. Mague, Chem. Data Collect. 17–18 (2018) 472.
[38] Bruker, A.P.E.X.3., SADABS, S.A.I.N.T. & SHELXTL. (2016) Madison, WI.
[39] G.M. Sheldrick, Acta Crystallogr. A 713 (2015) 3.
[40] G.M. Sheldrick, Acta Crystallogr. Sect. C: Cryst. Struct. Commun. 713 (2015) 3.
[41] D. Cremer, J.A. Pople, J. Am. Chem. Soc. 97 (1975) 1354.
[42] K. Brandenburg, H. Putz, Diamond, Crystal Impact GbR (2012).
[43] A.D. Becke, J. Chem. Phys. 98 (1993) 5648.
[44] C. Lee, W. Yang, R.G. Parr, Phys. Rev. B 37 (1988) 785.
[45] B. Miehlich, A. Savin, H. Stoll, H. Preuss, Chem. Phys. Lett. 157 (1989) 200.
[46] F. Weigend, R. Ahlrichs, Phys. Chem. Chem. Phys. 7 (2005) 3297.
[47] M.J. Frisch, G.W. Trucks, H.B. Schlegel, et al., Gaussian 16, Revision A.03., Gaussian, Inc., Wallingford, CT, 2016.
[48] A.J. Stone, J. Phys. Chem. A 121 (2017) 1531.
[49] M.A. Spackman, P.G. Byrom, Chem. Phys. Lett. 267 (1997) 215.
[50] J.J. McKinnon, M.A. Spackman, A.S. Mitchell, Acta Crystallogr. Sect. B 60 (2004) 627.
[51] M.A. Spackman, D. Jayatilaka, Cryst. Eng. Comm. 11 (2009) 19.
[52] M.J. Turner, J.J. McKinnon, S.K. Wolff, et al., CrystalExplorer17, University of Western Australia, Crawley, 2017.
[53] G.M. Morris, R. Huey, W. Lindstrom, M.F. Sanner, R.K. Belew, D.S. Goodsell, A.J. Olson, J. Comput. Chem. 30 (2009) 2785.
[54] B. Zhao, M.J. Bower, P.J. McDevitt, H. Zhao, S.T. Davis, K.O. Johanson, S.M. Green, N.O. Concha, B.B.S. Zhou, J. Biol. Chem. 277 (2002) 46609.
[55] D. Cremer, J.A. Pople, J. Am. Chem. Soc. 97 (1975) 1354.
[56] Chemcraft - graphical software for visualization of quantum chemistry computations. https://www.chemcraftprog.com.
[57] P. Geerlings, E.E. Chamorro, P.K. Chattaraj, F. De Proft, J.L. Gázquez, S. Liu, C. Morell, A. Toro Labbé, A. Vela, P. Ayers, Theor. Chem. Accouts 139 (2020) 36.
[58] M. Hagar, H.A. Ahmed, G. Aljohani, O.A. Alhaddad, Int. J. Mol. Sci. 21 (2020) 3922.
[59] A.R. Finkelmann, A.H. Göller, G. Schneider, Chem. Commun. 52 (2016) 681.